Chemically Powered Nanodimers

Gunnar Rückner and Raymond Kapral

Chemical Physics Theory Group, Department of Chemistry, University of Toronto, Toronto, Ontario M5S 3H6, Canada

(Received 3 January 2007; published 13 April 2007)

Self-propelled motion of a chemically powered nanodimer is discussed. The nanodimer comprises two linked spheres, one of which has equal interactions with A and B solvent species but catalyzes the reaction $A \rightarrow B$. The other sphere is not chemically active but interacts differently with the two species. The nonequilibrium concentration gradient generated at the catalytic end, in conjunction with the force difference at the noncatalytic end, leads to directed motion. The model mimics features of experimentally studied synthetic nanorod motion. Particle-based simulations and analytical estimates of the velocity provide insight into the nature of nanomotor directed motion.

DOI: 10.1103/PhysRevLett.98.150603 PACS numbers: 05.70.Ln, 02.70.Ns, 05.40.−a, 05.60.Cd

Self-propelled motion is common in biological systems. Molecular motors such as kinesin utilize chemical energy derived from the hydrolysis of ATP to induce conformational changes that lead to processive motion on microtubules [1]. Such directed motion plays a crucial role in active transport within the cell. Swimming bacteria such as *E. coli* use chemical energy to operate rotary molecular motors that drive the flagella which propel the cell [2]. These nano and micron-scaled objects operate in the regime of low Reynolds number hydrodynamics [3].

A much simpler class of synthetic nanoscale motors has been studied recently [4–6]. These motors are made from bimetallic Pt-Au nanorods immersed in a H_2O_2 solution. The catalytic reaction $2H_2O_2(\ell) \rightarrow O_2(g) + 2H_2O(\ell)$ occurs at the Pt end of the rod and is the power source for the motion. One plausible mechanism for motion involves the surface tension gradient due to O_2 adsorption on the nonreactive Au end. The mechanism is reminiscent of that for camphor boats where local changes in the surface tension of water drive the motion [7]. The molecular-level details of how O_2 generated at the Pt end of the nanorod leads to the propulsive force remain to be elucidated. Similarly, propulsion of spherical particles has been proposed to occur due to osmotic or other phoretic forces and an asymmetric distribution of reaction products in surface enzymatic reactions [8]. Synthetic nanomotors hold promise for applications including drug transport, chemical transport in microfluidic systems and pollution control. An understanding of the factors that control the locomotion is essential for the design of synthetic nanomotors.

In this Letter we examine the motion of a simple chemically powered nanomotor with many features akin to those responsible for the motion of synthetic nanorod motors. In contrast to many motor models [9], both the motor and the solvent are described at the particle level using a hybrid mesoscopic-molecular dynamics scheme [10]. The simplicity of the model allows us to analyze the mechanism of chemically powered directed motion in molecular detail. The study provides insight into how such motors can utilize chemical energy to produce directed motion.

Both synthetic and biological nanomotors must be able to function in a highly fluctuating molecular environment. Brownian motors where fluctuations are important have been the subject of numerous studies [11]. At the smallest length scales nanomotors must sense the molecular nature of the environment and in this regime continuum descriptions may not be applicable, motivating particle-based simulations.

We consider a nanodimer made from two spheres separated by a fixed distance R dissolved in a solvent of $N = N_A + N_B$ A and B molecules in a volume V. One dimer sphere (C) catalyzes the irreversible reaction $A + C \rightarrow B + C$, while the interactions with the noncatalytic sphere (N) do not lead to reaction (see Fig. 1). The A and B species interact with the nanodimer spheres through repulsive Lennard-Jones (LJ) potentials, $V_{C\alpha}$ and $V_{N\alpha}$, ($\alpha = A, B$), for the catalytic and noncatalytic spheres, respectively, with forms $V_{C\alpha}(r) = 4\epsilon_{C\alpha}[(\frac{\sigma_S}{r})^{12} - (\frac{\sigma_S}{r})^6 + \frac{1}{4}]$ for $r \leq r_c = 2^{1/6}\sigma_S$ and zero otherwise, with a similar expression for $V_{N\alpha}$. We take $V_{CA} = V_{CB} = V_{NA}$, characterized by the energy parameter ϵ_A and V_{NB} characterized by ϵ_B. The σ_S

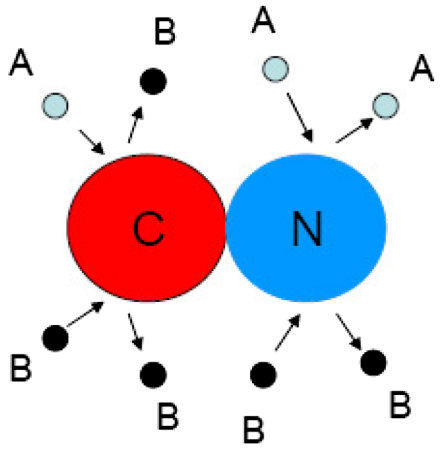

FIG. 1 (color online). Catalytic (C) and noncatalytic (N) dimer spheres and the collision events that occur on interaction of the A and B species with each sphere.

parameters are the same for all interactions. Whenever an A-type molecule enters the interaction distance $r < r_c$ it converts to B with probability p_R. The B molecules produced in the reaction interact differently with the catalytic and noncatalytic spheres. This model mimics generic features of synthetic nanorods: catalytic reactions occur on one end and the reaction product interacts differently with the catalytic and noncatalytic ends.

In our mesoscopic description, there are no interactions among the A and B solvent molecules; instead their interactions are accounted for by multiparticle collisions (MPC) [10]. Thus, the total potential energy of the system is

$$V(\mathbf{r}^{N_A}, \mathbf{r}^{N_B}) = \sum_{\alpha=A}^{B} \sum_{i=1}^{N_\alpha} [V_{C\alpha}(r_{i\alpha}) + V_{N\alpha}(r'_{i\alpha})]. \quad (1)$$

We use $\mathbf{r}$ to denote coordinates measured with the catalytic sphere as the origin, and $\mathbf{r}'$ coordinates measured with the noncatalytic sphere as the origin, so that $\mathbf{r}' = \mathbf{r} - \mathbf{R}$, where $\mathbf{R}$ is directed from the C to N spheres. The time evolution of the system is carried out using hybrid molecular dynamics-multiparticle collision (MD-MPC) dynamics [10] as follows: Using Eq. (1), Newton's equations are integrated for a time τ. At the discrete times τ multiparticle collisions among the solvent A and B molecules take place. To carry out the collisions, the volume V is partitioned into cells labeled by an index ξ and rotation operators $\hat{\omega}_\xi$, chosen at random from some set of rotation operators, are assigned to each cell at the time τ. If $\mathbf{V}_\xi$ is the center of mass velocity in cell ξ, the postcollision velocity $\mathbf{v}'_i$ of any particle i in the cell is given by $\mathbf{v}'_i = \mathbf{V}_\xi + \hat{\omega}_\xi(\mathbf{v}_i - \mathbf{V}_\xi)$, where $\mathbf{v}_i$ is the precollision velocity. This simple collision rule accounts for the effects of many real collisions. It conserves mass, momentum, and energy and preserves phase space volumes. The dynamics is microcanonical and the single particle distribution function relaxes to a Maxwellian distribution [10]. Thus, MPC dynamics possesses the important features of full MD. On macroscopic scales MPC dynamics yields the Navier-Stokes equations with transport coefficients determined by the collision rules [10,12,13]. Hydrodynamic interactions, which are important for nanodimer dynamics, are properly described [14].

We simulated the nanodimer motion for $\epsilon_A = 1$ and various values of ϵ_B. LJ units based on ϵ_A and σ are used throughout. The simulation parameters are as follows: The cubic volume V has linear dimension 32 and is divided into $32 \times 32 \times 32$ cells for the purpose of carrying out multiparticle collisions. To effect the multiparticle collisions we chose rotations by $\pm\pi/2$ about a randomly chosen axis. The total number of solvent molecules in the volume is 300 000 giving an average number density of $n_0 \approx 9$ particles/cell. The masses of the point-particle A and B species are $m = 1$. The nanodimer spheres have masses $m_S = 320$ and diameters $\sigma_S = 2$ so that the dimer is approximately neutrally buoyant. The dimer internuclear separation is held fixed at $R = 2\sigma_S + 0.5$ by a holonomic constraint in the equations of motion. The value of R insures that there are no discontinuous potential changes when B particles are produced in the reaction. The temperature is $T = 1/3$. Newton's equations were integrated using the velocity Verlet algorithm with a time step of $\Delta t = 0.01$. The multiparticle collision time is $\tau = 100\Delta t = 1$. Periodic boundary conditions were employed. Averages were computed from 100 realizations with Boltzmann sampling of initial conditions of trajectories of length 1000τ. Our simulations are microcanonical and the reaction $A \rightarrow B$ can produce a small change in T as a result of the change in the potential. This change is negligible for our large system.

Since the nanodimer is free to rotate, we compute the mean value of the dimer center of mass velocity projected along the instantaneous direction of the internuclear axis, $\langle\langle \mathbf{V}(t) \cdot \hat{\mathbf{R}}(t) \rangle\rangle \equiv V_z$, where the double angular brackets denote an average over time and realizations. Figure 2 plots the running time average $\langle \mathbf{V}(t) \cdot \hat{\mathbf{R}}(t) \rangle = \langle V_z \rangle(t)$ versus time for several values of ϵ_B and $\epsilon_A = 1$. Here the angle brackets denote an average over realizations. The figure shows that the chemical reaction at the catalytic end of the nanodimer does indeed produce directed motion whose sign depends on whether ϵ_B is greater or less than ϵ_A. For $\epsilon_B < \epsilon_A$ we find $V_z > 0$ ("forward drive") while for $\epsilon_B > \epsilon_A$ we find $V_z < 0$ ("reverse drive"). The directed motion can only occur if (a) there are different forces acting on the dimer spheres and (b) there is a nonequilibrium gradient in the B particle density. To confirm that the mechanism relies on the different forces that the B particles experience, the curve labeled A in Fig. 2 is for a nonreactive system with only A molecules. This is also equivalent to a reactive system with $\epsilon_A = \epsilon_B$ since reaction is simply a relabeling that has no effect on the forces. No nanodimer net motion is observed.

The existence of directed motion relies on the nonequilibrium density gradient of A and B species produced by the chemical reaction. Figure 3 is a snapshot of the solvent

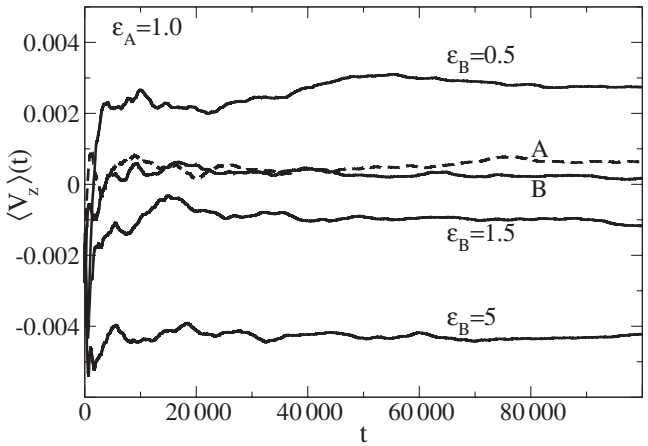

FIG. 2. Running average $\langle V_z \rangle(t)$, versus time (in units of the MD time step) for several values of ϵ_B. For curves A and B there is no directed motion (see text).

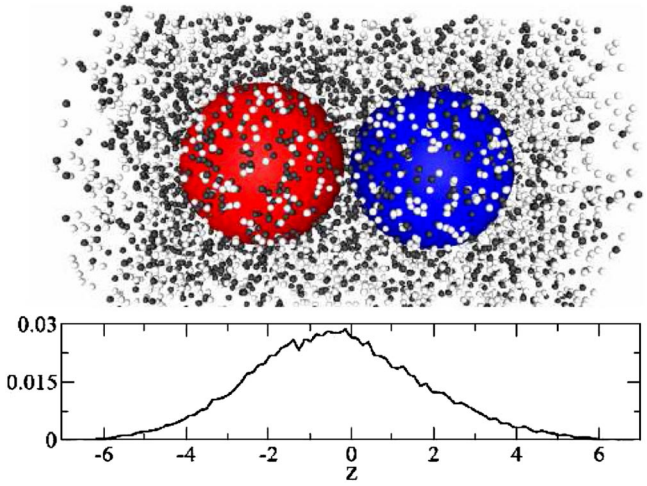

FIG. 3 (color online). Snapshot of the A (gray) and B (black) particles in the vicinity of the nanodimer in the quasi-steady-state regime. (lower panel) The average B density in a cylindrical shell versus z along the dimer bond.

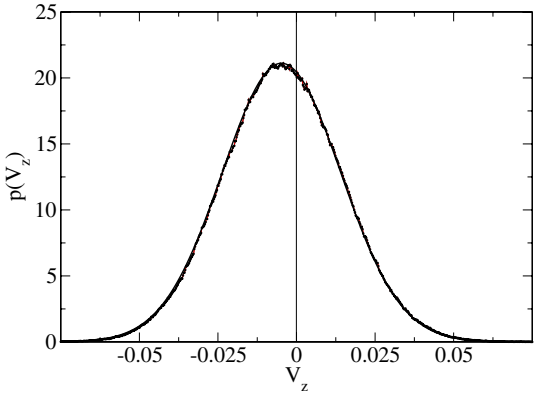

FIG. 4 (color online). Probability distribution function $p(V_z)$ of the center of mass velocity projected along the internuclear axis for $\epsilon_B = 5.0$. The solid curve is a fit to a Boltzmann distribution with mean velocity $V_z = -0.0048$.

configuration in the vicinity of the nanodimer in the quasi-steady-state regime. The local density of species B varies from high to low along the nanodimer internuclear axis from the C to N spheres. The density field is asymmetric due to scattering by the noncatalytic sphere (see lower panel). In the absence of such a nonequilibrium gradient there is no directed motion. Since the reaction at the C sphere is irreversible, nanodimer directed motion will cease when all A species have been converted to B. In the curve labeled B in Fig. 2, all solvent molecules were of B type. Thus, no chemical reaction occurs, although the B particles still have different interaction potentials with the C and N nanodimer spheres. There is no net directed motion confirming that a nonequilibrium gradient is necessary for the effect.

Nanodimer dynamics is strongly influenced by fluctuations as seen in Fig. 4, which shows the probability distribution of $\mathbf{V}\cdot\hat{\mathbf{R}} = V_z$. The mean nanodimer velocity is smaller than its standard deviation signalling the importance of fluctuations for these small motors. The dimer will also tumble as it moves. The reorientational relaxation time, $\tau_\theta \approx 4\pi\eta R^3/3k_BT$, is $\tau_\theta \approx 2000$ for our nanodimer so that for $\epsilon_B = 5.0$ the dimer will travel about 2–3 times its length before it reorients. Since τ_θ scales as R^3 tumbling will be strongly suppressed for longer dimers.

We now consider the factors that contribute to the force on the fixed nanodimer. The coordinate origin is the catalytic sphere center with the dimer along the z axis. Thus, $\mathbf{R} = R\hat{\mathbf{z}}$ and the total z component of the force is

$$\hat{\mathbf{z}}\cdot\mathbf{F} = -\sum_{\alpha=A}^{B}\sum_{i=1}^{N_\alpha}\left((\hat{\mathbf{z}}\cdot\mathbf{r}_{i\alpha})\frac{dV_{C\alpha}(r_{i\alpha})}{dr_{i\alpha}} + (\hat{\mathbf{z}}\cdot\mathbf{r}'_{i\alpha})\frac{dV_{N\alpha}(r'_{i\alpha})}{dr'_{i\alpha}}\right). \tag{2}$$

Introducing the local microscopic density field for species α, $\rho_\alpha(\mathbf{r};\mathbf{r}^{N_\alpha}) = \sum_{i=1}^{N_\alpha}\delta(\mathbf{r}-\mathbf{r}_{i\alpha})$, and its average over a steady state or equilibrium distribution denoted by $\rho_\alpha(\mathbf{r}) = \langle\sum_{i=1}^{N_\alpha}\delta(\mathbf{r}-\mathbf{r}_{i\alpha})\rangle$, the average z component of the force is

$$\langle\hat{\mathbf{z}}\cdot\mathbf{F}\rangle = -\sum_{\alpha=A}^{B}\int d\mathbf{r}\rho_\alpha(\mathbf{r})(\hat{\mathbf{z}}\cdot\hat{\mathbf{r}})\frac{dV_{C\alpha}(r)}{dr} - \sum_{\alpha=A}^{B}\int d\mathbf{r}'\rho_\alpha(\mathbf{r}'+\mathbf{R})(\hat{\mathbf{z}}\cdot\hat{\mathbf{r}}')\frac{dV_{N\alpha}(r')}{dr'}. \tag{3}$$

The first and second integrals have their coordinate systems centered on the catalytic C and noncatalytic N spheres, respectively.

To obtain the velocity we assume a steady state where the force due to the reaction is balanced by the frictional force: $\zeta V_z = \langle\hat{\mathbf{z}}\cdot\mathbf{F}\rangle$. Since the diffusion coefficient is related to the friction by $D = k_BT/\zeta = 1/\beta\zeta$, we have

$$V_z = D\langle\hat{\mathbf{z}}\cdot\beta\mathbf{F}\rangle. \tag{4}$$

The calculation hinges on knowing the nonequilibrium steady state densities. First, consider the forms of the equilibrium densities. Since there are no solvent-solvent forces the equilibrium density of A is given by

$$\rho_A^{\mathrm{eq}}(\mathbf{r}_A) = n_A e^{-\beta[V_{CA}(r_A)+V_{NA}(|\mathbf{r}_A-R\hat{\mathbf{z}}|)]}, \tag{5}$$

where $n_A = N_A/V$ is the density of A. A similar expression can be written for the B density. It is easy to see that if this expression is substituted into Eq. (3), the result is zero in view of the central forms of the LJ potentials. There is no directed motion in equilibrium.

To estimate the nonequilibrium density we make use of the solution of the diffusion equation

$$\frac{\partial n_A(r,t)}{\partial t} = D_A\nabla^2 n_A(r,t), \tag{6}$$

with a radiation boundary condition (BC) at the catalytic sphere, ignoring, for simplicity, the presence of the noncatalytic sphere. Assuming that the BC is applied outside a boundary layer lying in the range $\sigma_C \le r \le R_0$, the radia-

tion BC is $k_{f0}n_A(R_0, t) = 4\pi R_0^2 D_A \hat{\mathbf{r}} \cdot \nabla n_A(R_0, t)$. Thus, a suitable choice is $R_0 = r_c$. The density far from the catalytic sphere is $n_A^0 = \text{const}$. The steady state solution is

$$n_A(r) = n_A^0\left(1 - \frac{k_{f0}}{k_{f0} + k_D}\frac{R_0}{r}\right), \tag{7}$$

where $k_D = 4\pi R_0 D_A$. The rate constant for processes within the boundary layer is $k_{f0} = p_R \sigma_C^2 (8\pi k_B T/m)^{1/2}$, where p_R probability of reaction, taken to be unity in our study [15]. Since $n_B(r) + n_A(r) = n_A^0$, $n_B(r) = n_A^0[k_{f0}/(k_{f0} + k_D)](R_0/r)$.

From Eq. (5), the uniform number density n_A changes locally as a result of the potential appearing in the Boltzmann factor. The potentials are cutoff at $2^{1/6}\sigma_S$. Thus, in the nonequilibrium steady state we may replace the constant density in Eq. (5) by the steady-state density from the diffusion calculation, at least for distances outside the interaction range, so that

$$\rho_A(\mathbf{r}) \approx n_A(\mathbf{r}) e^{-\beta[V_{CA}(r_A) + V_{NA}(|\mathbf{r}_A - R\hat{\mathbf{z}}|)]}, \tag{8}$$

with a similar equation for the B density. Since the forces $dV_{C\alpha}/dr$ are zero outside the cutoff distance r_c centered on the C sphere, we can write Eq. (4) as

$$\frac{V_z}{D\beta} = -\int d\mathbf{r}' n_A(|\mathbf{r}' + R\hat{\mathbf{z}}|) e^{-\beta V_{NA}(r')}(\hat{\mathbf{z}} \cdot \hat{\mathbf{r}}')\frac{dV_{NA}(r')}{dr'} - \int d\mathbf{r}' n_B(|\mathbf{r}' + R\hat{\mathbf{z}}|) e^{-\beta V_{NB}(r_A)}(\hat{\mathbf{z}} \cdot \hat{\mathbf{r}}')\frac{dV_{NB}(r')}{dr'}. \tag{9}$$

The steady state density from Eq. (7) should apply outside the noncatalytic sphere; thus, we take $n_A(|\mathbf{r}' + R\hat{\mathbf{z}}|) \approx n_A(|r_c\hat{\mathbf{r}}' + R\hat{\mathbf{z}}|)$ to compute the integrals. (A similar expression holds for the B density.) Using the explicit forms of the densities we find

$$V_z = Dn_A^0 \frac{k_{f0}}{k_{f0} + k_D} R_0\left(\int d\hat{\mathbf{r}}' |r_c\hat{\mathbf{r}}' + R\hat{\mathbf{z}}|^{-1}\right) \times \int_0^{r_c} dr' r'^2 \left[\frac{d\beta V_{NA}(r')}{dr'} e^{-\beta V_{NA}(r')} - \frac{d\beta V_{NB}(r')}{dr'} e^{-\beta V_{NB}(r')}\right]. \tag{10}$$

The angular integral can be performed analytically and radial integral numerically to obtain estimates of the nanodimer velocity. The diffusion coefficient of the center of mass of the nanodimer was determined from the mean square displacement and found to be $D = 0.0048$. The following results were obtained (numbers in parentheses are the simulation results determined from fits of $p(V_z)$ to Boltzmann distributions): $V_z = 0.0036(0.0028)$ for $\epsilon_B = 0.5$; $V_z = 0.0(0.0)$ for $\epsilon_B = 1.0$; $V_z = -0.0018(-0.0013)$ for $\epsilon_B = 1.5$; $V_z = -0.0072(-0.0048)$ for $\epsilon_B = 5.0$. This analysis captures the trends seen in the simulations, in particular the change from "forward to reverse drive" as ϵ_B varies, and shows the factors that are needed to produce directed motion.

Experimental techniques exist for fabricating colloidal homo and heterodoublets whose constituent spheres have nanoscale dimensions [16,17]. It should be possible to construct nanodimer motors in order to study directed motion in regimes where fluctuations are important and macroscopic concepts may lose their validity.

This work was supported in part by a grant from the Natural Sciences and Engineering Research Council of Canada. We would like to thank G. Ozin for discussions that stimulated this investigation.

[1] R. D. Vale and R. A. Milligan, Science **288**, 88 (2000).
[2] H. Berg, *E. coli in Motion* (Springer, New York, 2003).
[3] E. M. Purcell, Am. J. Phys. **45**, 3 (1977).
[4] W. F. Paxton, K. C. Kistler, C. C. Olmeda, A. Sen, S. K. St. Angelo, Y. Cao, T. E. Mallouk, P. E. Lammert, and V. H. Crespi, J. Am. Chem. Soc. **126**, 13 424 (2004).
[5] W. F. Paxton, A. Sen, and T. E. Mallouk, Chem. Eur. J. **11**, 6462 (2005).
[6] A. Fournier-Bidoz, A. C. Arsenault, I. Manners, and G. A. Ozin, Chem. Commun. (Cambridge) 441 (2005).
[7] L. Rayleigh, Proc. R. Soc. London **47**, 364 (1889).
[8] R. Golestanian, T. B. Liverpool, and A. Ajdari, Phys. Rev. Lett. **94**, 220801 (2005).
[9] One exception is the motor in C. Van den Broeck, R. Kawai, and P. Meurs, Phys. Rev. Lett. **93**, 090601 (2004) where the solvent is treated by molecular dynamics.
[10] A. Malevanets and R. Kapral, J. Chem. Phys. **110**, 8605 (1999); **112**, 7260 (2000).
[11] For a review see, for example, P. Reimann, Phys. Rep. **361**, 57 (2002).
[12] T. Ihle and D. M. Kroll, Phys. Rev. E **63**, 020201 (2001).
[13] N. Kikuchi, C. M. Pooley, J. F. Ryder, and J. M. Yeomans, J. Chem. Phys. **119**, 6388 (2003).
[14] S. H. Lee and R. Kapral, J. Chem. Phys. **122**, 214916 (2005).
[15] K. Tucci and R. Kapral, J. Chem. Phys. **120**, 8262 (2004).
[16] A. M. Yake, R. A. Panella, C. E. Snyder, and D. Velegol, Langmuir **22**, 9135 (2006).
[17] M. Ibisate, Z. Zou, and Y. Xia, Adv. Funct. Mater. **16**, 1627 (2006).